SPE 29099

Logically Rectangular Mixed Methods for Darcy Flow on General Geometry

Todd Arbogast, Philip T. Keenan, Mary F. Wheeler, SPE Member, and Ivan Yotov,
Rice University, Houston, Texas.

ABSTRACT

We consider an expanded mixed finite element formulation (cell centered finite differences) for Darcy flow with a tensor absolute permeability. The reservoir can be geometrically general with internal features, but the computational domain is rectangular. The method is defined on a curvilinear grid that need not be orthogonal, obtained by mapping the rectangular, computational grid. The original flow problem becomes a similar problem with a modified permeability on the computational grid. Quadrature rules turn the mixed method into a cell-centered finite difference method with a 9 point stencil in 2-D and 19 in 3-D.

As shown by theory and experiment, if the modified permeability on the computational domain is smooth, then the convergence rate is optimal and both pressure and velocity are superconvergent at certain points. If not, Lagrange multiplier pressures can be introduced on boundaries of elements so that optimal convergence is retained. This modification presents only small changes in the solution process; in fact, the same parallel domain decomposition algorithms can be applied with little or no change to the code if the modified permeability is smooth over the subdomains.

This Lagrange multiplier procedure can be used to extend the difference scheme to multi-block domains, and to give a coupling with unstructured grids. In all cases, the mixed formulation is locally conservative. Computational results illustrate the advantage and convergence of this method.

1. INTRODUCTION

We develop a numerical scheme for Darcy flow with a tensor

References at end of paper

permeability on a geometrically general domain Ω in $\mathbf{R}^d$ ($d = 2$ or 3). Although our results generalize to multiphase problems, for simplicity we consider the single phase flow problem in which we solve for the pressure p and the velocity $\mathbf{u}$ satisfying

$$\nabla \cdot \mathbf{u} = q, \qquad \text{in } \Omega, \qquad (1.1a)$$

$$\mathbf{u} = -K\nabla p, \quad \text{in } \Omega, \qquad (1.1b)$$

$$\mathbf{u} \cdot \nu = 0, \qquad \text{on } \partial\Omega, \qquad (1.1c)$$

where K is the absolute permeability tensor divided by viscosity and ν denotes the unit normal to the domain boundary, $\partial\Omega$. Tensor permeabilities frequently arise from homogenization or in up-scaling of displacement processes in heterogeneous reservoirs. Our techniques apply to problems with more general boundary conditions, as well.

Our numerical scheme is based on mixed finite element methods, because they conserve mass locally and give a good approximation of the flux variable. However, mixed methods can be difficult to implement directly. In particular, the algebraic system that arises is a saddle-point problem which involves solving simultaneously for pressure and velocities.

By using special quadrature rules for evaluating the integrals, Russell and Wheeler [1] showed that the standard cell-centered finite difference method was equivalent to the lowest order, RT_0 mixed method [2] on strictly rectangular grids provided that the permeability is diagonal. Thus, the RT_0 mixed method can be easily implemented as a five or seven point finite difference method. Weiser and Wheeler [3] obtained superconvergence results for this scheme; that is, if h is the maximum grid spacing, both the pressure and

velocity are approximated to order h^2 at certain points. A Galerkin method will approximate the velocity only to order h.

To solve the flow problem with a tensor coefficient on a fairly geometrically general domain, we need to develop a new scheme. We will not sacrifice the ease of implementation, the accuracy, or the local mass conservation property of the approximation. We present in the next section the expanded mixed finite element method that is the basis of our scheme [4, 5, 6]. Extensions to the expanded hybrid formulation are also discussed. The hybrid formulation involves introducing Lagrange multipliers on the boundaries of elements or subdomains on which the components of the tensor are discontinuous. This is an important modification to obtain higher order accurate fluxes.

Our main requirement is that there be a smooth mapping F of a rectangular, computational domain $\hat{\Omega}$ onto the reservoir domain Ω. Given a rectangular grid $\hat{\mathcal{T}}_h$ on $\hat{\Omega}$, F defines a smooth, logically rectangular, curvilinear grid $\mathcal{T}_h$ on Ω (see Fig. 1). The Jacobian matrix of F is $DF = \left(\partial F_i / \partial \hat{x}_j\right)$, and the Jacobian of the mapping is $J = |\det(DF)|$. (Mapping techniques have been employed in the aerospace industry for many years [7]. Sophisticated software packages are commercially available for creating F and its Jacobian matrix.) Our work here differs from [8] in that we do not require the mesh to be orthogonal.
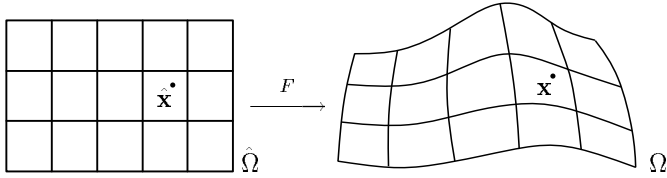

Fig. 1. The computational domain $\hat{\Omega}$
and the physical domain Ω.

We derive our finite difference procedure [4, 6] in Section 3, and summarize our convergence results [4, 5] in Section 4. Computational experiments are given in Section 5, including experimental convergence results for tensor coefficient problems, an example of a parallel domain decomposition substructuring algorithm for solving the expanded hybrid formulation, and a tracer calculation on a general domain. Extensions to multi-block grids, coupling with unstructured grids, and conclusions are discussed in Section 6.

2. THE EXPANDED AND EXPANDED HYBRID MIXED FINITE ELEMENT METHODS ON GENERAL GEOMETRY

We first define the expanded mixed finite element method. Following [4] and [5], we introduce an unknown $\tilde{\mathbf{u}}$, called the adjusted pressure gradient, such that

$$M\tilde{\mathbf{u}} = -\nabla p, \qquad (2.1a)$$

$$\mathbf{u} = KM\tilde{\mathbf{u}}, \qquad (2.1b)$$

where $M = J(DF^{-1})^T DF^{-1}$. Note that M is a symmetric, positive definite matrix. It is introduced to simplify the

computations significantly, after mapping to the rectangular grid on $\hat{\Omega}$.

To define the RT_0 mixed space on the curvilinear grid, we need first the standard definition of this space on rectangles [2]. Let $\hat{V}_h$ and $\hat{W}_h$ be the velocity and the pressure space, respectively. On any rectangular element $\hat{E} \in \hat{\mathcal{T}}_h$,

$$\hat{V}_h(\hat{E}) = \left\{ (\alpha_1 x_1 + \beta_1, \alpha_2 x_2 + \beta_2, \alpha_3 x_3 + \beta_3)^T : \alpha_i, \beta_i \in \mathbf{R} \right\},$$
$$\hat{W}_h(\hat{E}) = \left\{ \alpha : \alpha \in \mathbf{R} \right\}$$

(where the last component of $\hat{V}_h(\hat{E})$ should be deleted if $d = 2$). Then,

$$\hat{V}_h = \big\{ \hat{\mathbf{v}} = (v_1, v_2, v_3) : \ \hat{\mathbf{v}}|_{\hat{E}} \in \hat{V}_h(\hat{E}) \text{ for all } \hat{E} \in \hat{\mathcal{T}}_h,$$
$$\text{and each } v_i \text{ is continuous in}$$
$$\text{the } i\text{th coordinate direction} \big\},$$
$$\hat{W}_h = \big\{ \hat{w} : \hat{w}|_{\hat{E}} \in \hat{W}_h(\hat{E}) \text{ for all } \hat{E} \in \hat{\mathcal{T}}_h \big\};$$

thus, if $\hat{\nu}$ denotes the unit normal direction, $\hat{\mathbf{v}} \cdot \hat{\nu}$ is a well defined constant on the edges (if $d = 2$) or faces (if $d = 3$) of each element $\hat{E}$, and $\hat{w}$ is piecewise discontinuous constant. We use the standard nodal basis, where for $\hat{V}_h$, the nodes are at the midpoints of the edges or faces of the elements, and for $\hat{W}_h$, the nodes are at the midpoints of the elements (cell-centers).

To properly incorporate the boundary condition (1.1c), we need to introduce Lagrange multiplier pressures along $\partial\Omega$; thus, on any element edge or face $\hat{e}$, let

$$\hat{\Lambda}_h(\hat{e}) = \left\{ \alpha : \alpha \in \mathbf{R} \right\}$$

and then define

$$\hat{\Lambda}_h^\partial = \big\{ \hat{\mu} : \hat{\mu}|_{\hat{e}} \in \hat{\Lambda}_h(\hat{e}) \text{ for all edges or faces}$$
$$\hat{e} \text{ of } \hat{E} \in \hat{\mathcal{T}}_h \text{ contained in } \partial\Omega \big\}.$$

The nodal points are the centers of the edges or faces.

Let V_h, W_h, and Λ_h^∂ be the RT_0 spaces on $\mathcal{T}_h$, defined as follows [9, 10]. For each $\hat{\mathbf{v}} \in \hat{V}_h$, $\hat{w} \in \hat{W}_h$, and $\hat{\mu} \in \hat{\Lambda}_h^\partial$, we define $\mathbf{v} \in V_h$, $w \in W_h$, and $\mu \in \Lambda_h^\partial$ at $F(\hat{\mathbf{x}}) = \mathbf{x} \in \Omega$ by

$$\mathbf{v}(\mathbf{x}) = \frac{1}{J(\hat{\mathbf{x}})} DF(\hat{\mathbf{x}})\hat{\mathbf{v}}(\hat{\mathbf{x}}), \qquad (2.2a)$$

$$w(\mathbf{x}) = \hat{w}(\hat{\mathbf{x}}), \qquad (2.2b)$$

$$\mu(\mathbf{x}) = \hat{\mu}(\hat{\mathbf{x}}). \qquad (2.2c)$$

The velocity space is defined by the Piola transformation; it preserves the normal component of the velocity across the element boundaries and is therefore locally mass conservative. The key property is that $\nabla \cdot \mathbf{v} = \frac{1}{J}\hat{\nabla} \cdot \hat{\mathbf{v}}$.

We have the following mixed formulation for approximating the flow equation (1.1). Find $\mathbf{u}_h \in V_h$, $\tilde{\mathbf{u}}_h \in V_h$, $p_h \in W_h$, and $\lambda_h \in \Lambda_h^\partial$ such that

$$\int_E \nabla \cdot \mathbf{u}_h \, dx = \int_E q \, dx, \qquad E \in \mathcal{T}_h, \quad (2.3a)$$

$$\int_\Omega M \tilde{\mathbf{u}}_h \cdot \mathbf{v} \, dx$$
$$= \int_\Omega p_h \nabla \cdot \mathbf{v} \, dx - \int_{\partial \Omega} \lambda_h \mathbf{v} \cdot \nu \, ds, \quad \mathbf{v} \in V_h, \quad (2.3b)$$

$$\int_\Omega M \mathbf{u}_h \cdot \mathbf{v} \, dx = \int_\Omega M K M \tilde{\mathbf{u}}_h \cdot \mathbf{v} \, dx, \quad \mathbf{v} \in V_h, \quad (2.3c)$$

$$\int_{\partial \Omega} \mathbf{u}_h \cdot \nu \, \mu \, dx = 0, \qquad \mu \in \Lambda_h^\partial. \quad (2.3d)$$

The existence and uniqueness of a solution is shown in [4, 5].

We now transform (2.3) to the rectangular, computational domain by the map F. The Piola transform (2.2a), (2.2b), (2.2c), and the definition of M (2.1) imply that

$$\int_{\hat{E}} \hat{\nabla} \cdot \hat{\mathbf{u}}_h \, d\hat{x} = \int_E q \, dx = \int_{\hat{E}} \hat{q} J \, d\hat{x}, \qquad \hat{E} \in \hat{\mathcal{T}}_h, \quad (2.4a)$$

$$\int_{\hat{\Omega}} \hat{\tilde{\mathbf{u}}}_h \cdot \hat{\mathbf{v}} \, d\hat{x}$$
$$= \int_{\hat{\Omega}} \hat{p}_h \hat{\nabla} \cdot \hat{\mathbf{v}} \, d\hat{x} - \int_{\partial \hat{\Omega}} \hat{\lambda}_h \hat{\mathbf{v}} \cdot \hat{\nu} \, d\hat{s}, \quad \hat{\mathbf{v}} \in \hat{V}_h, \quad (2.4b)$$

$$\int_{\hat{\Omega}} \hat{\mathbf{u}}_h \cdot \hat{\mathbf{v}} \, d\hat{x}$$
$$= \int_{\hat{\Omega}} J D F^{-1} K (D F^{-1})^T \hat{\tilde{\mathbf{u}}}_h \cdot \hat{\mathbf{v}} \, d\hat{x}, \quad \hat{\mathbf{v}} \in \hat{V}_h, \quad (2.4c)$$

$$\int_{\partial \hat{\Omega}} \hat{\mathbf{u}}_h \cdot \hat{\nu} \, \hat{\mu} \, d\hat{x} = 0, \qquad \hat{\mu} \in \hat{\Lambda}_h^\partial, \quad (2.4d)$$

where $\hat{q}(\hat{\mathbf{x}}) = q(F(\hat{\mathbf{x}}))$. Note that (2.4) is similar to the original problem (2.3) with $M = I$ and the modified tensor coefficient

$$\mathcal{K} = J D F^{-1} K (D F^{-1})^T. \quad (2.5)$$

All computations are performed on the rectangular grid of $\hat{\Omega}$; we recover the true pressure and velocity on Ω using (2.2).

The expanded hybrid method involves adding additional Lagrange multipliers on internal element edges or faces, and relaxing the continuity constraints on V_h. We define the fullest case, where Lagrange multipliers are added to every element edge or face. Let

$$\hat{V}_h^D = \left\{ \hat{\mathbf{v}} = (v_1, v_2, v_3) : \hat{\mathbf{v}}|_{\hat{E}} \in \hat{V}_h(\hat{E}) \text{ for all } \hat{E} \in \hat{\mathcal{T}}_h \right\},$$

$$\hat{\Lambda}_h = \left\{ \hat{\mu} : \hat{\mu}|_{\hat{e}} \in \hat{\Lambda}_h(\hat{e}) \text{ for all edges or faces } \hat{e} \text{ of } \hat{E} \in \hat{\mathcal{T}}_h \right\},$$

and then define V_h^D and Λ_h analogously by (2.2a) and (2.2c). Equation (2.3) is modified by requiring that V_h and Λ_h^∂ be replaced by V_h^D and Λ_h, respectively, and (2.3b) and (2.3d)

be replaced by

$$\int_E M \tilde{\mathbf{u}}_h \cdot \mathbf{v} \, dx$$
$$= \int_E p_h \nabla \cdot \mathbf{v} \, dx - \int_{\partial E} \lambda_h \mathbf{v} \cdot \nu \, ds, \quad \mathbf{v} \in V_h(E), \quad (2.3b')$$

$$\sum_{E \in \mathcal{T}_h} \int_{\partial E} \mathbf{u}_h \cdot \nu \, \mu \, ds = 0, \qquad \mu \in \Lambda_h. \quad (2.3d')$$

The latter equation insures continuity of the internal fluxes; thus, although for symmetry we ask only that $\mathbf{u} \in V_h^D$, in fact, $\mathbf{u} \in V_h$. Equation (2.4) is modified analogously.

In practice, Lagrange multipliers should be introduced only on a coarse grid or on the boundaries of subdomains. As shown in Section 5, employing Lagrange multipliers is useful in treating flow problems in which components of the tensor permeability are discontinuous and in applying non-overlapping or substructuring domain decomposition linear solvers. In the former case it should be noted that if $\mathcal{K}$ is not smooth on $\hat{e}$ of $\hat{E} \in \hat{\mathcal{T}}_h$, then $\hat{\tilde{\mathbf{u}}} \cdot \hat{\nu} = -\hat{\nabla}\hat{p} \cdot \hat{\nu}$ is also not smooth there. Hence $\hat{\tilde{\mathbf{u}}}$ should be approximated in the discontinuous space V_h^D near $\hat{e}$.

3. THE CELL-CENTERED FINITE DIFFERENCE METHOD

To simplify the finite element method (2.4), we use special quadrature rules to approximate the integrals. The four divergence and boundary integrals can be computed exactly, since the divergence and normal component of any $\hat{\mathbf{v}} \in \hat{V}_h$ are piece-wise constants. The trapezoidal rule is used for evaluating the three integrals over Ω involving a vector-vector product. This enables us to express $\hat{\mathbf{u}}_h$ and $\hat{\tilde{\mathbf{u}}}_h$ in terms of $\hat{p}_h$ and $\hat{\lambda}_h$, and therefore obtain a single equation for the pressure. Herein, we describe this stencil for $d = 2$; a straightforward generalization gives the stencil for $d = 3$.

We need some relatively standard cell-centered finite difference notation. Denote the grid points by

$$(\hat{x}_{i+1/2}, \hat{y}_{j+1/2}), \quad i = 0, ..., N_1, \; j = 0, ..., N_2,$$

and define, for $i = 1, ..., N_1$ and $j = 1, ..., N_2$,

$$\hat{x}_i = \tfrac{1}{2}(\hat{x}_{i+1/2} + \hat{x}_{i-1/2}), \qquad \hat{y}_j = \tfrac{1}{2}(\hat{y}_{j+1/2} + \hat{y}_{j-1/2}),$$
$$\hat{h}_i^{\hat{x}} = \hat{x}_{i+1/2} - \hat{x}_{i-1/2}, \qquad \hat{h}_j^{\hat{y}} = \hat{y}_{j+1/2} - \hat{y}_{j-1/2}.$$

We write $\mathbf{v} = (v^{\hat{x}}, v^{\hat{y}})$ for $\mathbf{v} \in \mathbf{R}^2$. For any function $g(\hat{x}, \hat{y})$, let g_{ij} denote $g(\hat{x}_i, \hat{y}_j)$, $g_{i+1/2,j}$ denote $g(\hat{x}_{i+1/2}, \hat{y}_j)$, etc.

As illustrated in Fig. 2, the finite difference stencil is constructed as follows. If $\hat{\mathbf{v}}$ in (2.4b) is the basis function at an interior node $(i + 1/2, j)$ or $(i, j + 1/2)$, then

$$\hat{\tilde{u}}^{\hat{x}}_{h,i+1/2,j} = -\frac{\hat{p}_{h,i+1,j} - \hat{p}_{h,i,j}}{\frac{1}{2}(\hat{h}_i^{\hat{x}} + \hat{h}_{i+1}^{\hat{x}})}, \quad (3.1a)$$
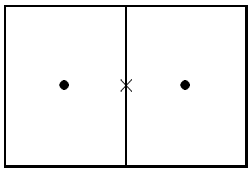
$$\hat{\tilde{u}}^{\hat{y}}_{h,i,j+1/2} = -\frac{\hat{p}_{h,i,j+1} - \hat{p}_{h,i,j}}{\frac{1}{2}(\hat{h}_j^{\hat{y}} + \hat{h}_{j+1}^{\hat{y}})}, \quad (3.1b)$$

which is a finite difference approximation of $\hat{\tilde{\mathbf{u}}} = -\hat{\nabla}\hat{p}$ (at the boundary, $\hat{\lambda}_h$ replaces $\hat{p}_h$—see (3.4) below). The same choice of $\hat{\mathbf{v}}$ in (2.4c) gives

$$\hat{u}^{\hat{x}}_{h,i+1/2,j}$$

$$= \frac{1}{2}\left[(\mathcal{K}_{11})_{i+1/2,j-1/2} + (\mathcal{K}_{11})_{i+1/2,j+1/2}\right]\hat{\tilde{u}}^{\hat{x}}_{h,i+1/2,j}$$

$$+ \frac{1}{2(\hat{h}^{\hat{x}}_i + \hat{h}^{\hat{x}}_{i+1})}\left\{\left[(\mathcal{K}_{12})_{i+1/2,j-1/2}\hat{\tilde{u}}^{\hat{y}}_{h,i+1,j-1/2}\right.\right.$$

$$\left. + (\mathcal{K}_{12})_{i+1/2,j+1/2}\hat{\tilde{u}}^{\hat{y}}_{h,i+1,j+1/2}\right]\hat{h}^{\hat{x}}_{i+1}$$

$$+ \left[(\mathcal{K}_{12})_{i+1/2,j-1/2}\hat{\tilde{u}}^{\hat{y}}_{h,i,j-1/2}\right.$$

$$\left.\left. + (\mathcal{K}_{12})_{i+1/2,j+1/2}\hat{\tilde{u}}^{\hat{y}}_{h,i,j+1/2}\right]\hat{h}^{\hat{x}}_i\right\}, \qquad (3.2)$$

with a similar expression for $\hat{u}^{\hat{y}}_{h,i,j+1/2}$ (slightly modified by dropping a few terms near $\partial\Omega$); this is a finite difference approximation of $\hat{\mathbf{u}} = \mathcal{K}\hat{\tilde{\mathbf{u}}}$. Finally, for $E = E_{ij}$ in (2.4a), we have

$$\left\{\frac{\hat{u}^{\hat{x}}_{h,i+1/2,j} - \hat{u}^{\hat{x}}_{h,i-1/2,j}}{\hat{h}^{\hat{x}}_i} + \frac{\hat{u}^{\hat{y}}_{h,i,j+1/2} - \hat{u}^{\hat{y}}_{h,i,j-1/2}}{\hat{h}^{\hat{y}}_j}\right\}\hat{h}^{\hat{x}}_i\hat{h}^{\hat{y}}_j$$

$$= \int_{\hat{E}_{ij}}\hat{q}J\,d\hat{x} = \int_{E_{ij}}q\,dx. \qquad (3.3)$$

(a)

(b)

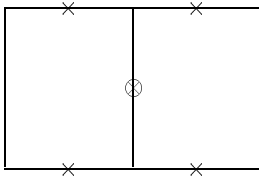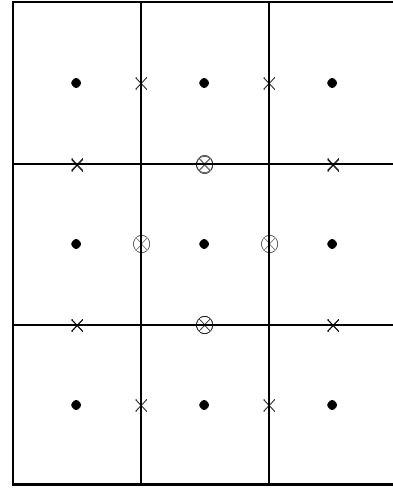$\otimes = \mathbf{u}_h$ and $\tilde{\mathbf{u}}_h$

$\times = \tilde{\mathbf{u}}_h$ only

$\bullet = p_h$

(c)

Fig. 2. Nodal points for the standard basis functions ($d = 2$).
(a) Stencil for the dependence of $\tilde{\mathbf{u}}_h$ on p_h.
(b) Stencil for the dependence of $\mathbf{u}_h$ on $\tilde{\mathbf{u}}_h$.
(c) Stencil for the pressure p_h.

The combination of (3.1), (3.2), and (3.3) gives our cell-centered finite difference stencil for the pressures $\hat{p}$ and $\hat{\lambda}$ approximating the elliptic equation $-\hat{\nabla}\cdot\mathcal{K}\hat{\nabla}\hat{p} = \hat{q}J$. This in turn is an approximation of the original problem (1.1) through (2.2). The stencil is 9 points in two dimensions and 19 points in three dimensions.

The hybrid formulation involves modifying (3.1) by replacing $\hat{p}_{h,i+1,j}$ or $\hat{p}_{h,i,j+1}$ by the appropriate Lagrange multiplier. For example, we now have both a left and right value of $\hat{\tilde{u}}^{\hat{x}}_h$ at an interior node $(i+1/2,j)$, and

$$\hat{\tilde{u}}^{\hat{x}}_{h,(i+1/2)^-,j} = -\frac{\hat{\lambda}_{h,i+1/2,j} - \hat{p}_{h,i,j}}{\frac{1}{2}\hat{h}^{\hat{x}}_i}, \qquad (3.4a)$$

$$\hat{\tilde{u}}^{\hat{x}}_{h,(i+1/2)^+,j} = -\frac{\hat{p}_{h,i+1,j} - \hat{\lambda}_{h,i+1/2,j}}{\frac{1}{2}\hat{h}^{\hat{x}}_{i+1}}. \qquad (3.4b)$$

Again, a finite difference stencil results, but it is now a combination of cell-centered and face-centered pressures. In fact $\hat{p}_h$ can be eliminated in terms of $\hat{\lambda}_h$, leaving only the face-centered pressures.

4. SOME CONVERGENCE RESULTS

Let $\|\cdot\|$ denote the L^2-norm; that is, for a scalar or vector function φ,

$$\|\varphi\| = \sqrt{\int_\Omega |\varphi(\mathbf{x})|^2\,dx}.$$

Let $\|\|\cdot\|\|_{M,S}$, where S is a subset of Ω, denote the L^2-norm approximated by the midpoint quadrature rule over

the mesh on S defined either directly or as induced by F from the computational domain. The proof of the following theorem is given in [4] and [5]. This result holds for general boundary conditions, including mixed or Robin conditions.

Theorem. *Let Ω^* be a fixed, closed domain strictly contained in Ω. For the cell-centered finite difference scheme (3.1)–(3.3), there exists a constant C depending on the solution and the smoothness of F and $\mathcal{K}$, but independent of the maximum grid spacing h, such that*

$$\|\mathbf{u} - \mathbf{u}_h\| + \|\tilde{\mathbf{u}} - \tilde{\mathbf{u}}_h\| \le Ch,$$

$$|||\mathbf{u} - \mathbf{u}_h|||_{M,\Omega} + |||\tilde{\mathbf{u}} - \tilde{\mathbf{u}}_h|||_{M,\Omega} \le Ch^{3/2},$$

$$|||\mathbf{u} - \mathbf{u}_h|||_{M,\Omega^*} + |||\tilde{\mathbf{u}} - \tilde{\mathbf{u}}_h|||_{M,\Omega^*} \le Ch^2,$$

$$\|p - p_h\| \le Ch,$$

$$|||p - p_h|||_{M,\Omega} \le Ch^2,$$

$$\|\nabla \cdot (\mathbf{u} - \mathbf{u}_h)\| \le Ch.$$

This theorem implies optimal order convergence in the L^2-norms, and superconvergence in L^2 for the computed pressure and velocity at the cell-centers. The velocity exhibits better superconvergence away from the boundary of the domain. Furthermore, the normal component of the flux at the midpoints of the edges or faces is also superconvergent in the interior of the domain (see [4]).

Tests show that the predicted rates of convergence are obtained by the method, including the superconvergence [4, 5].

5. SOME COMPUTATIONAL RESULTS

In this section we present numerical results which demonstrate (1) experimental rates of convergence, (2) a scalable parallel domain decomposition algorithm for solving the expanded hybrid mixed finite element method, and (3) a tracer problem on a real field site.

5.1. Some experimental rates of convergence. In exhibiting experimental rates of convergence, we present two examples. The first is a two dimensional case similar to [11; Fig. 7], but using a logically rectangular mesh of quadrilaterals rather than triangles. The mesh is shown in Fig. 3. As in [11], the mesh conforms to a low permeability streak in which a full tensor coefficient K is chosen so that flow is reduced along the streak and sharply reduced perpendicular to the streak. K is chosen to be the identity tensor outside the streak. The streak is only one mesh element wide. We impose no flow boundary conditions along the top and bottom of the unit square, and unit flow in through the left boundary and out through the right.
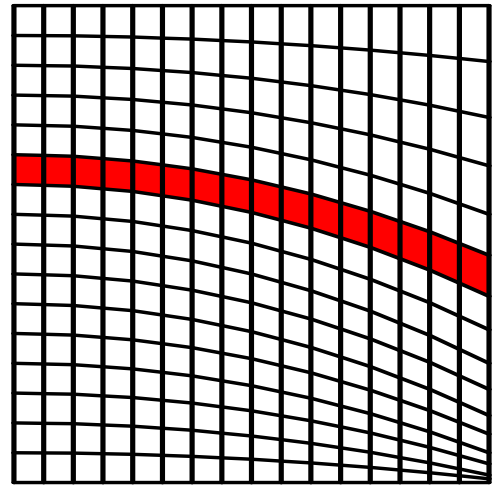

Fig. 3. Mesh of quadrilaterals.

"Weather-vanes" of the resulting velocity field, approximated by the mixed finite element method on 256 elements, is shown in Fig. 4. If the streak were absent, the velocity would be uniformly equal to $(1, 0)^T$. Subtracting this constant vector from the computed velocity field shows the perturbation caused by the streak, illustrated in Fig. 5, in which the residual vectors have been magnified by a factor of 5 compared to Fig. 4. Relatively little fluid can cross the low permeability streak, but conservation of mass and the constant flow rate per unit length of boundary require some fluid which enters below the streak to migrate into the top region. Fluid in the top layer must speed up so that enough can get through the large outflow boundary. In the bottom layer, fluid must slow down since there is less room for it to exit. This creates the circular pattern in Fig. 5.
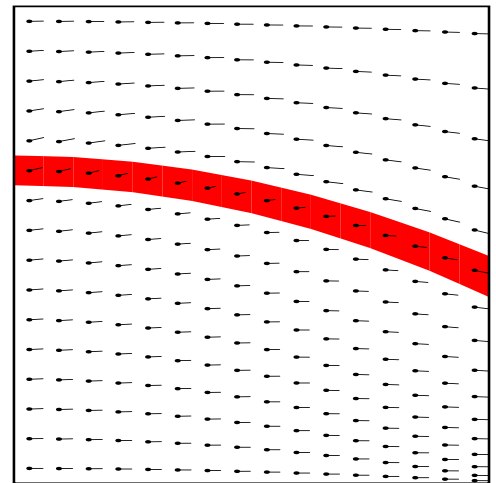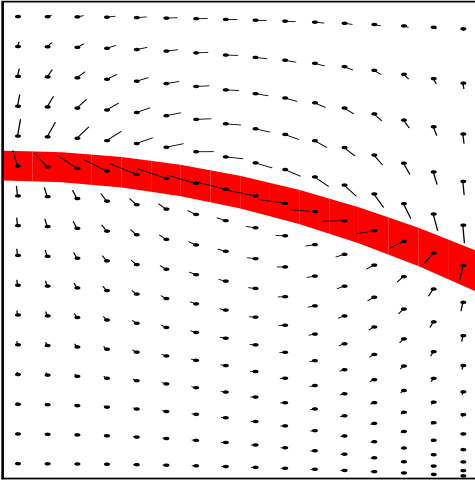

Fig. 4. Velocity field.

Fig. 5. Residual velocity field magnified 5 times.

Our other convergence example is in three spatial dimensions. We present a convergence study in a situation with a known analytic solution. The domain is the union of the unit cube and its reflection into negative x values; that is, $[-1, 1] \times [0, 1] \times [0, 1]$. We define K to be the identity for negative x and

$$K = \begin{pmatrix} 5 & 4 & 4 \\ 4 & 5 & 4 \\ 4 & 4 & 5 \end{pmatrix}.$$

for positive x. We constructed a pressure solution that is quadratic on each sub-cube, continuous at $x = 0$, and has continuous normal component of flux at $x = 0$. We then solved

$$-\nabla \cdot (K(\mathbf{x})\nabla p(\mathbf{x})) = f(\mathbf{x}),$$

where f is a different constant in each of the two sub-cubes, and used pressure boundary conditions matching the constructed target solution.

We repeatedly refined the mesh and calculated pressure and velocity, and compared them to the target values. Table 1 presents the discrete L^2 norms of the errors evaluated at the element centers. We see that both pressure and velocity are super-convergent. The maximum error in the normal fluxes is shown in the final column; it converges like $O(h)$. These results use the expanded mixed method with Lagrange multipliers along the interface $x = 0$.

Table 1. Pressure and velocity errors.

$1/h$	$\|\|\|p - p_h\|\|\|_{M,\Omega}$	$\|\|\|\mathbf{u} - \mathbf{u}_h\|\|\|_{M,\Omega}$	$\|\mathbf{u} - \mathbf{u}_h\|_\infty$
2	0.1070	1.089	2.52
4	0.0272	0.409	1.31
8	0.0069	0.141	0.66
16	0.0017	0.048	0.33
Rate	$0.7\,h^2$	$4.3\,h^{1.5}$	$6.6h$

If the Lagrange multipliers are removed, the L^2 errors grow substantially and the maximum normal flux error fails to converge, as seen in Table 2. It is interesting to note that

to visual accuracy, the results without Lagrange multipliers seem reasonable when viewing plots of the solution and the flux in a corresponding 2-D example. This shows the importance of checking the convergence rate of numerical methods used in non-smooth contexts by comparison to known analytic solutions.

Table 2. Errors without interface Lagrange multipliers.

$1/h$	$\|\|\|p - p_h\|\|\|_{M,\Omega}$	$\|\|\|\mathbf{u} - \mathbf{u}_h\|\|\|_{M,\Omega}$	$\|\mathbf{u} - \mathbf{u}_h\|_\infty$
2	0.5031	9.50	20.4
4	0.2691	5.84	23.0
8	0.1340	3.51	24.9
16	0.0648	2.12	26.0
Rate	$1.3\,h$	$20\,h^{0.75}$	$O(1)$

5.2. A domain decomposition algorithm for the expanded mixed method. To solve the linear system that arises in the discretization, we employ a substructuring or domain decomposition algorithm which was introduced by Glowinski and Wheeler [12]. The method requires solving only local problems and is in fact a hybrid formulation over subdomains.

In addition to its advantage on parallel machines, this method allows one to handle accurately problems with a discontinuous permeability tensor. In such a case, the gradient of the pressure $\tilde{\mathbf{u}}$ is also discontinuous. Approximating it with a continuous function does not give good results; however, accuracy is retained if the hybrid form of the expanded mixed method is used. In that case, the pressure is also computed on the edges or faces of the elements and its gradient is approximated in an element by element discontinuous space.

The domain decomposition method introduces pressure unknowns (Lagrange multipliers) along the subdomain interface and is equivalent to a partial hybridization of the original method. Therefore it is very accurate if the discontinuity of the coefficient lies along a subdomain boundary. To efficiently solve the interface problem on a distributed memory, parallel computer system, the balancing preconditioner defined by Cowsar, Mandel, and Wheeler [13] has been employed. (Theoretical and computational results exhibiting the almost linear scalability of this preconditioner are given in [13].) Numerical tests are presented below.

We solve a problem on the unit cube in 3D. The permeability and the true pressure field are chosen such that the normal flux is continuous:

$$K = \begin{cases} K_1, & 0 < x < 0.5, \\ K_2, & 0.5 < x < 1, \end{cases}$$

$$K_1 = \begin{pmatrix} 14/9 & 7/9 & 0 \\ 7/9 & 2 & 0 \\ 0 & 0 & 2 \end{pmatrix}, \quad K_2 = \begin{pmatrix} 1 & 1/2 & 0 \\ 1/2 & 2 & 0 \\ 0 & 0 & 2 \end{pmatrix},$$

$$p = \begin{cases} 1 - x^3, & 0 < x < 0.5, \\ \frac{7}{6}(1 - x^2), & 0.5 < x < 1. \end{cases}$$

Dirichlet or Neumann boundary conditions can be specified on any part of the boundary. For this test we specify pressure on the faces $x = 0$ and $x = 1$ and flux on the rest of the boundary. The domain decomposition is $2 \times 1 \times 1$ (two subdomains in the x-direction). The pressure and velocity error as well as the estimated least squares convergence rates are given in Table 3. Since the solution is constant in y and z, the mesh has been refined only in the x-direction. Quadratic convergence is observed for both variables. (We suspect that since p does not vary in y or z, the velocity convergence is somewhat better than is usually observed, such as in the previous subsection.) If no domain decomposition is used, the convergence deteriorates due to a loss of accuracy along the discontinuity. The results are presented in Table 4.

Fig. 6. The true grid with the low permeability region.

Table 3. Errors with domain decomposition.

$1/h_x$	$\|\|\|p - p_h\|\|\|_{M,\Omega}$	$\|\|\|\mathbf{u} - \mathbf{u}_h\|\|\|_{M,\Omega}$
4	9.75E-3	3.92E-2
8	2.46E-3	9.81E-3
16	6.18E-4	2.45E-3
32	1.55E-4	6.13E-4
64	3.87E-5	1.53E-4
128	9.66E-6	3.83E-5
Rate	$O(h^2)$	$O(h^2)$

Table 4. Errors without domain decomposition.

$1/h_x$	$\|\|\|p - p_h\|\|\|_{M,\Omega}$	$\|\|\|\mathbf{u} - \mathbf{u}_h\|\|\|_{M,\Omega}$
4	1.00E-2	4.39E-2
8	2.99E-3	1.27E-2
16	1.04E-3	4.17E-3
32	4.30E-4	1.63E-3
64	1.97E-4	7.19E-4
128	9.51E-5	3.40E-4
Rate	$O(h^{1.33})$	$O(h^{1.40})$

Fig. 7. The computational domain with the low permeability region.

A uniform pressure drop occurs from the back face (Haw Ridge) to the front face (White Oak Lake and Copper Ridge); no-flow is specified across the other faces. Pressure contours are given in Fig. 8. Tracer concentration fronts at four equally spaced times are shown on Fig. 9. The flow through the low permeability region is very slow; also the streamlines along the left edge are longer then in the rest of the domain so the flow is slower there.

5.3 A single phase flow and transport example on general geometry.
In the next example we demonstrate tracer injection at the WAG–6 (Waste Area Grouping #6) site of the Oak Ridge National Laboratory (ORNL). The transport equation is solved by using the characteristics-mixed method of Arbogast and Wheeler [14, 15] (see also [6] for its generalization to general geometry). The permeability is isotropic but discontinuous. There is a low permeability region where its value is 20 times smaller then in the rest of the domain. Fig. 6–7 show the true grid and the computational grid with the low permeability streak.
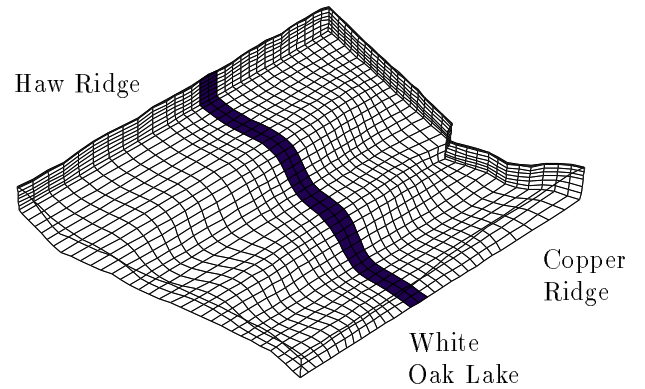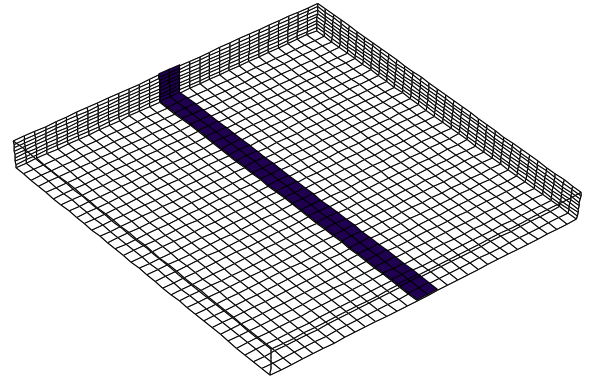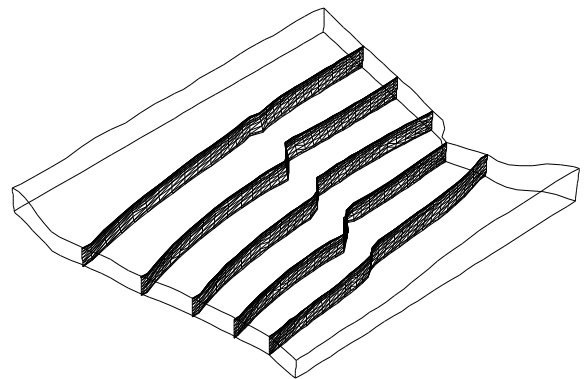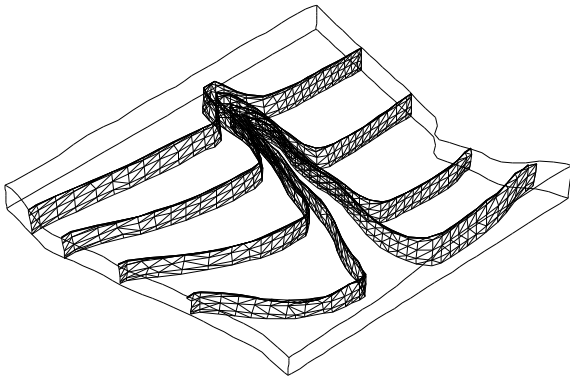

Fig. 8. Pressure contours.

Fig. 9. Tracer concentration fronts with the low permeability region.

6. EXTENSIONS AND CONCLUSIONS

We have presented a cell-centered finite difference mixed method that is locally mass conservative and highly accurate, especially for the velocity. General geometry can be handled by a multi-block approach. The physical domain is divided into a union of subdomains. Each of the subdomains is mapped smoothly to a rectangle; their union constitutes the computational domain. This is a standard technique in the aerospace industry (so many commercial gridding codes are available).

The equations are then mapped from the physical to the computational domain. The net result is a simple transformation of the tensor permeability and the multiplication of certain other terms by the Jacobian factor. A rectangular grid is put on the computational domain, but the physical grid need not be orthogonal. The scheme is easily implemented, since the data structures need only reflect the rectangular, computational grids.

Lagrange multiplier pressures must be introduced on the common boundaries of adjacent rectangles in the multi-block case. This approach can also be used to couple structured and unstructured grids (see [16]), and to handle grid refinements.

Theoretical results including superconvergence have been established in the case of single phase flow, a single rectangular computational domain, and a smooth map and permeability. Theoretical analysis of the multi-block case is currently under investigation. Computational results verify these theoretical results. Moreover, we observed that the introduction of Lagrange multiplier pressures on boundaries where either the map or the permeability is not smooth recovers convergence and even some of the superconvergence.

Scalable and efficient, parallel domain decomposition algorithms such as described in [13, 17] have been formulated that are applicable for solving the resulting finite difference equations.

Extensions of these finite difference mixed method techniques to multiphase flow are straight forward. One of the authors, Wheeler with C. Dawson, C. San Soucie, and H. Klie

are currently applying this approach to a black oil simulator. These techniques have also been extended to triangles [16].

NOMENCLATURE

d	Spatial dimension (2 or 3)
DF	Jacobian matrix of F.
ds	Differential of surface length (if d=2) or area (if d=3)
dx	Differential of area (if d=2) or volume (if d=3)
e	Edge (if d=2) or face (if d=3) of a finite element
E	Finite element
F	Mapping between the computational and physical domains
h	Maximum grid spacing
i	Index in x-direction
j	Index in y-direction
J	Absolute value of the determinant of the Jacobian of F.
K	Permeability tensor divided by the viscosity
$\mathcal{K}$	The transformed permeability tensor divided by the viscosity
M	Mapping dependent adjustment to the negative pressure gradient
p	Pressure
q	External well sources and sinks
$\mathbf{R}$	Set of real numbers
RT_0	The lowest order Raviart-Thomas mixed finite element function space
$\mathcal{T}_h$	Grid partition into elements
$\mathbf{u}$	Darcy velocity
$\tilde{\mathbf{u}}$	Adjusted pressure gradient
$\mathbf{v}$	Velocity test function
V_h	Velocity finite element function space
V_h^D	The discontinuous flux, velocity finite element function space
w	Pressure test function
W_h	Pressure finite element function space
$\mathbf{x}$	Spatial point
(x, y, z)	Spatial point
(x_1, x_2, x_3)	Spatial point
∂E	Boundary of the finite element E
$\partial \Omega$	Boundary of the reservoir
λ	Lagrange pressure
Λ_h	Lagrange pressure finite element function space
Λ_h^∂	Lagrange pressure finite element function space on the boundary only
μ	Lagrange pressure test function
ν	Outer unit normal vector
Ω	Reservoir domain
$\hat{\cdot}$	Quantity as seen on the computational domain
$\cdot_h$	Discrete quantity
$\| \cdot \|$	L^2 (root mean square) norm
$\|\| \cdot \|\|_M$	Discrete L^2 norm approximated by the midpoint rule
$\| \cdot \|_\infty$	Maximum norm

ACKNOWLEDGMENTS

REFERENCES

[1] Russell, T.F., and Wheeler, M.F.: "Finite element and finite difference methods for continuous flows in porous media," in The Mathematics of Reservoir Simulation, Frontiers in Applied Mathematics 1, Ewing, R.E., ed., Society for Industrial and Applied Mathematics, Philadelphia (1983) Chapter II, pp. 35–106.

[2] Raviart, R.A., and Thomas, J.M.: "A mixed finite element method for 2nd order elliptic problems," in Mathematical Aspects of the Finite Element Method, Lecture Notes in Math. 606, Springer-Verlag, New York (1977) pp. 292–315.

[3] Weiser, A., and Wheeler, M.F.: "On convergence of block-centered finite-differences for elliptic problems," SIAM J. Numerical Analysis, v. 25 (1988) pp. 351–375.

[4] Arbogast, T., Dawson, C., Keenan, P., Wheeler, M.F., and Yotov, I.: "Implementation of mixed finite element methods for elliptic equations on general geometry" (in preparation).

[5] Arbogast, T., Wheeler, M.F., and Yotov, I.: "Mixed finite elements for elliptic problems with tensor coefficients as cell-centered finite differences" (in preparation).

[6] Arbogast, T., Wheeler, M.F., and Yotov, I.: "Logically rectangular mixed methods for groundwater flow and transport on general geometry," in Computational Methods in Water Resources X, Vol. 1, Peters, A., et al., eds., Kluwer Academic Publishers, Dordrecht, The Netherlands (1994) pp. 149–156.

[7] Thompson, J., Warsi, Z.U.A., and Mastin, C.W.: Numerical Grid Generation, North Holland (1985).

[8] Sharpe, H.N.: "Validation of an Adaptive, Orthogonal, Curvilinear Gridding Procedure for Reservoir Simulation," SPE 25262, 12th Symposium on Reservoir Simulation, New Orleans (1993) pp. 333-343.

[9] Thomas, J.M.: "Sur l'analyse numérique des méthodes d'éléments finis hybrides et mixtes," Thèse d'Etat, Université Pierre et Marie Curie (1977).

[10] Brezzi, F., and Fortin, M.: Mixed and hybrid finite element methods, Springer-Verlag, New York (1991).

[11] Durlofsky, L.J.: "Accuracy of mixed and control volume finite element approximations to Darcy velocity and related quantities," Water Resources Research, v. 30 (1994) pp. 965–973.

[12] Glowinski, R., and Wheeler, M.F.: "Domain decomposition and mixed finite element methods for elliptic problems," in the Proceedings of the First International Symposium on Domain Decomposition Methods for Partial Differential Equations, Glowinski, R., et al., eds., Society for Industrial and Applied Mathematics, Philadelphia (1987).

[13] Cowsar, L.C., Mandel, J., and Wheeler, M.F.: "Balancing domain decomposition for Mixed Finite Elements," Mathematics of Computation (in press).

[14] Arbogast, T., and Wheeler, M.F.: "A characteristics-mixed finite element method for advection dominated transport problems," SIAM J. Numerical Analysis (in press).

[15] Arbogast, T., Chilakapati, A., and Wheeler, M.F.: "A characteristic-mixed method for contaminant transport and miscible displacement," in Computational Methods in Water Resources IX, Vol. 1: Numerical Methods in Water Resources, Russell, T.F., et al., eds., Computational Mechanics Publications, Southampton, U.K. (1992) pp. 77–84.

[16] Arbogast, T., Dawson, C.N., and Keenan, P.T.: "Efficient mixed methods for groundwater flow on triangular or tetrahedral meshes," in Computational Methods in Water Resources X, Vol. 1 Peters, A., et al., eds., Kluwer Academic Publishers, Dordrecht, The Netherlands (1994) pp. 3–10.

[17] Cowsar, L.C., Weiser, A., and Wheeler, M.F., "Parallel multigrid and domain decomposition algorithms for elliptic equations", Fifth Symposium on Domain Decomposition Methods for Partial Differential Equations, Keyes, D., et al., eds., Society for Industrial and Applied Mathematics, Philadelphia (1991) pp. 37–386.